Research Article | Vol. 29, No. 23 / 8 Nov 2021 / Optics Express 37081
Optics EXPRESS

Electromagnetic induction imaging: signal detection based on tuned-dressed optical magnetometry

GIUSEPPE BEVILACQUA,[1] VALERIO BIANCALANA,[1,*] YORDANKA DANCHEVA,[2,3] ALESSANDRO FREGOSI,[2,4] GAETANO NAPOLI,[5] AND ANTONIO VIGILANTE[2]

[1] *Dipartimento di Ingegneria dell'Informazione e Scienze Matematiche - DIISM, Università di Siena – Via Roma 56, 53100 Siena, Italy*
[2] *Dipartimento di Scienze Fisiche, della Terra e dell'Ambiente - DSFTA, Università di Siena – Via Roma 56, 53100 Siena, Italy*
[3] *Currently with Aerospazio Tecnologie – Rapolano (Siena), Italy*
[4] *CNR - Istituto Nazionale di Ottica – via Moruzzi 1, 56124 Pisa, Italy*
[5] *Dipartimento di Matematica e Fisica "Ennio De Giorgi" Università del Salento – 73100 Lecce, Italy*
[*] *valerio.biancalana@unisi.it*

Abstract: A recently introduced tuning-dressed scheme makes a Bell and Bloom magnetometer suited to detect weak variations of a radio-frequency (RF) magnetic field. We envisage the application of such innovative detection scheme as an alternative (or rather as a complement) to RF atomic magnetometers in electromagnetic-induction-imaging apparatuses.

1. Introduction

In 2001, Griffiths [1] proposed an imaging technique based on inferring one or more of the three passive electromagnetic properties (conductivity σ, permittivity ϵ and permeability μ) to produce images on the basis of the response to a position dependent oscillating magnetic field. Several denominations are used to identify this kind of methodologies, among which electromagnetic induction imaging (EII) [2], electro-magnetic tomograhy (EMT) [3], magnetic induction tomography (MIT) [4,5], and also mutual inductance tomography (same acronym) [6], the latter three stressing the potential of the technique to provide 3D mapping. A review on the subject was recently authored by Ma and Soleimani [7].

As a general feature, the technique uses an AC magnetic field (primary field) to excite eddy currents in the specimen. The secondary magnetic field generated by those currents is then detected and analyzed. A variety of approaches can be applied to detect the secondary field. Beside inductive detectors based on the Faraday's induction law (pick-up coils, possibly arranged in arrays), more advanced devices based on magnetometric sensors have been proposed to extend the bandwidth and/or to improve the sensitivity, at expense of larger cost and complexity. Among the latter, all-optical [8] and radio-frequency [9] atomic magnetometers (including cold-atom magnetometers [10,11]), as well as nitrogen vacancy magnetometers [12] have been successfully applied. In similar applications, the potential of eddy current detectors based on superconducting quantum interference [13,14] and on giant magnetoresistance [15–17] has been demonstrated.

Magnetometers can detect and record in-phase (ϵ dependent) and out-of-phase (σ dependent) response of specimens subjected to an excitation radio-frequency field B_{RF}. The response obtained while scanning the position of a sample with respect to the field generator and detector enables the registration of 2D maps. The possibility of varying the B_{RF} frequency (and correspondingly the skin depth in the specimen) has implications in the development of instrumentation with 3D (tomographic) capabilities.

#437930 https://doi.org/10.1364/OE.437930
Journal © 2021 Received 15 Jul 2021; revised 1 Sep 2021; accepted 19 Sep 2021; published 25 Oct 2021

Optics EXPRESS

Optical magnetometers, in the so-called radio-frequency (RF) implementation [9,18,19] are excellent detectors of weak (variation of) magnetic fields oscillating at a resonant frequency and hence constitute favourite detectors for EII, particularly in the case of low-conductivity and/or small-size specimens.

This led recently to important steps toward high resolution EII of weakly conductive materials. Appositely developed RF magnetometers with opportune field-specimen arrangement, [20,21], demonstrated a sensitivity sufficient to detect and characterize sub S m^{-1} conductive material in small size (5 ml) samples, despite the operation in unshielded environment [2].

Such specification level makes the technique suited to develop tools for medical diagnostics [22], where the negligible invasivity of EII represents a valuable attractive, but the low-conductivity and the need of high spatial resolution constitute a severe requirement.

This work considers the potential of a peculiar configuration of a Bell&Bloom (BB) magnetometer as a detector of eddy currents induced in small and/or weakly conductive specimens, which could be eventually used to produce maps in 2D or 3D scans.

While the basic principle of operation (detection of a secondary magnetic field) is shared with the above mentioned research, the proposed sensor works with an arrangement that does not require resonant conditions for the time-dependent excitation field. The proposed arrangement can constitute an alternative as well as a complement to the commonly used RF magnetometers.

The standard BB implementation of atomic magnetometers is based on optically pumping atoms into a given Zeeman sublevel (typically with a maximum magnetic number along the quantization axis defined by the pump light wavevector) that is not stationary due to the presence of a transverse magnetic field.

In the usual picture of the BB operation, the macroscopic magnetization precesses around the magnetic field direction and it is periodically reinforced when its orientation is along the optical axis of the pump beam. The periodic reinforcement is obtained by modulating the pump radiation –its intensity, polarization or wavelength– synchronously with the precession. A weak and unmodulated probe radiation interrogates the evolution of the atomic state and produces an output signal whose dynamics is driven by the field under measurement.

The presence of time dependent field can modify the spin dynamics also in non-resonant conditions. As an example, in conventional BB magnetometry, slow-varying magnetic field variations, oriented along the bias field direction, are detected with a high sensitivity. Field variations along perpendicular directions produce some signal, as well, but with a second-order response [23].

Interesting dynamic responses of precessing spins are observed in a different regime, namely in the case of an intense fast-varying magnetic field. In particular, a strong magnetic field oscillating along the probe-beam axis (i.e. transversely to the static one) at a frequency much above the resonance may effectively freeze the atomic precession, according with a phenomenon originally studied in the late Sixties [24] and generally known as *magnetic dressing*.

In a recent work [25], we have demonstrated that the dressing phenomenon can be deeply tuned by the application of a secondary (and much weaker) field that oscillates at the same frequency –or at a low-order harmonic– of the dressing one, perpendicularly to the latter. Among the peculiarities of such tuned-dressed configuration, we pointed out that the system shows a remarkable response to variations of the amplitude and/or of the phase of the tuning field. This work investigates with a proof-of-principle experiment the potential of such a tuning-dressing apparatus to detect tiny field variations due to eddy currents induced by the tuning field.

2. Experimental setup

The experimental setup is built around a BB magnetometer making use of cesium thermal vapor in a centimetric, gas buffered cell. The atomic vapour is synchronously pumped by D_1 radiation (at mW/cm^2 irradiance) and polarimetrically probed by a weak (at μW/cm^2 irradiance) D_2

Optics EXPRESS

radiation, co-propagating with the pump one along the x direction, further details can be found in Ref. [26].

The atomic sample is merged in a constant field at μT level (let its direction be z) oriented perpendicularly to the laser beams. This static field B_0 is obtained by partially compensating the environmental magnetic field. The task is accomplished by means of three large size (180 cm) mutually orthogonal Helmholtz pairs. Additional adjustable quadrupoles let improve the field homogeneity.

The tuning-dressing effect [25] occurs when two phase-related oscillating fields (B_D and B_t) are applied along x to dress the atoms, and along y to tune the dressing effect, respectively. A solenoidal coil (11 cm in length and 4 cm in diameter) surrounding the cell generates B_D and a small (millimetric) solenoid wound on a ferrite nucleus generates B_t. The interaction geometry is sketched in Fig. 1.

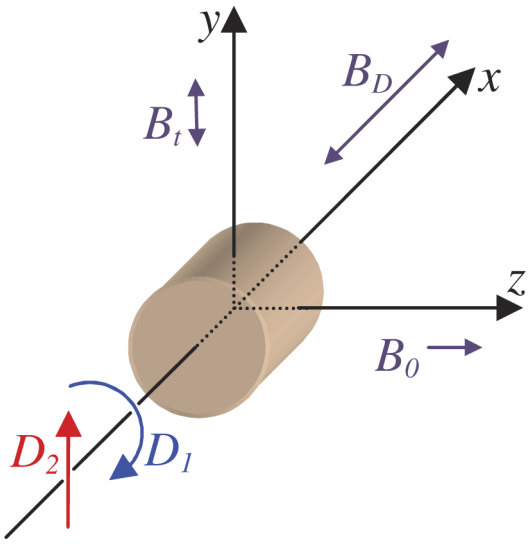

Fig. 1. Magnetic field and laser beams geometry. Circularly polarized D_1 pump radiation and linearly polarized D_2 probe radiation propagate along x, which is the same direction of a strong oscillating (dressing) field B_D. A weaker (tuning) field B_t oscillates along y synchronously with B_D; a weak static field B_0 is oriented along z.

The B_D and B_t coils are supplied by two waveform generators (Agilent 33250A) phase-locked to each other. Series capacitors help to adapt the impedances, and a linear amplifier can be used to enhance the B_t amplitude. Each of these coils has 10 Ohm series resistor to precisely monitor the current phases and amplitudes via a 16 bit, 500 kS/s DAQ card (NI 6346).

The tuning-dressed phenomenon occurs and is well modeled and characterized for a tuning-field frequency ω_t that is an integer multiple of the dressing frequency ω_D ($\omega_t = p\omega_D$). It is worth stressing that, in the considered application, switching among different p values may enable fast and relevant variations of the skin depth, which in EII applications may constitute an interesting feature.

The coil-specimen-sensor geometry is sketched in Fig. 2. The used specimens are one or more Aluminum disks of assigned thickness d, diverse radii R, centered on the y axis, and lying on a xz plane between the B_t generator and the atomic sensor. The experimental results reported in this work are obtained with a = 40 mm, b = 130 mm, d = 30 μm, and R ranging from 12 mm to 175 mm. In this proof-of-concept experiment, these values are chosen on the basis of fortuitous constraints of the available setup. In real imaging applications, all of them could be selected in

Optics EXPRESS

view of optimizing the detection performance, in terms of sensitivity and/or spatial resolution. In application to EII mapping, the spatial resolution would be mainly determined by the lowest among the parameters a and b and by either the C_t size or the sensor size, respectively. Thus further reducing a and the coil size would be a good strategy to improve the spatial resolution, similarly to cases in which different detection methods are used. At the same time, a smaller b would help improving the sample-sensor coupling and hence the detection efficiency. In addition, at the expense of using specially designed coil sets to generate the primary field, the spatial resolution could be improved by using field focusing techniques [27].

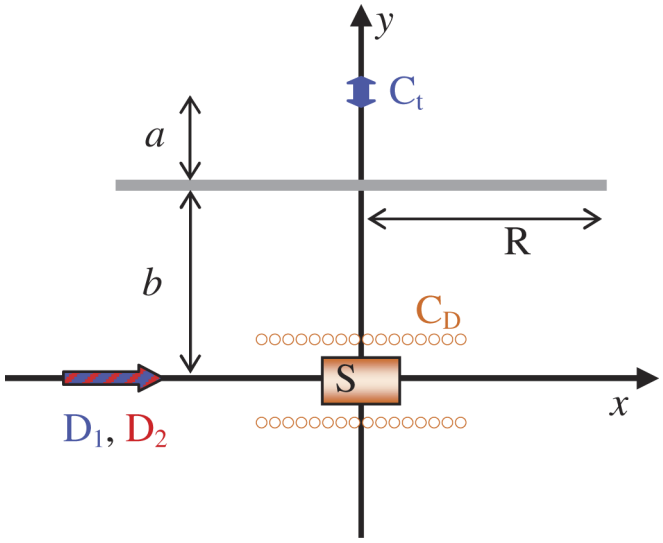

Fig. 2. Relative positions of specimen, sensor, and tuning/dressing field sources. The specimen is a circular disk of radius R (thick grey line), which is parallel to the xz plane and is centered on the y axis, at a quote $y = b$ over the sensor S. A solenoidal coil C_D surrounds S and produces a homogeneous field B_D along the x axis. The latter coincides with the optical axis of the pump and probe lasers D_1 and D_2. A small dipolar source C_t located on the y axis at distance a from the specimen (and $a + b$ from the sensor) produces a tuning field B_t which is oriented along y on the sensor, and excites tangential eddy currents in the disk. Those currents modify both the amplitude and the phase of the tuning field on S.

The eddy currents induced in the conductive disks modify the amplitude and the phase of B_t in the sensor location. As summarized in Sec.3., both these parameters play a role in shifting the effective Larmor frequency, and this is the key feature at the basis of the proposed detection technique.

3. Effective Larmor frequency

As shown and discussed in the Ref. [25], a magnetic field that oscillates in the direction perpendicular to both the transverse static field B_0 and the longitudinal dressing field B_D at a frequency p times larger than that of the dressing field, modifies the effective Larmor frequency according to

$$\Omega_L = \gamma \left[B_0 J_0(\xi) + B_t J_p(\xi) \sin(\phi) \right], \tag{1}$$

if p is an odd integer, and to

$$\Omega_L = \gamma \sqrt{[B_0 J_0(\xi)]^2 + \left[B_t J_p(\xi) \cos(\phi) \right]^2}, \tag{2}$$

Optics EXPRESS

if it is an even one. Here, γ is the atomic gyromagnetic factor ($\gamma \approx 3.5$ Hz/nT for Cesium), and the argument ξ is set by the amplitude of the dressing field B_D and by its frequency ω_D according to

$$\xi = \frac{\gamma B_D}{\omega_D}. \tag{3}$$

The validity of the eqs. 1 and 2 requires that

$$\xi \gg \frac{\gamma B_t}{\omega_D}, \frac{\omega_0}{\omega_D}. \tag{4}$$

In the measurements shown in this paper, the tuning field oscillates at the same frequency of B_D (i.e. $p = 1$), while both its amplitude and phase vary either due to different waveform-generator settings or to the presence of conductive samples placed in the proximity of the field source and of the sensor. In particular, assuming that $\phi = \varphi - \theta$, where φ is the relative phase of the two RF generators and θ is the dephasing caused by the eddy currents in the specimen, the effective Larmor frequency can be expressed as

$$f = \frac{\gamma}{2\pi}\left[J_0(\xi)B_0 + J_1(\xi)B_t \sin\phi\right] = f_0 + A\sin(\varphi - \theta), \tag{5}$$

where f_0 is the dressed frequency in absence of the tuning field. Beside causing the dephasing θ, the eddy currents attenuate B_t, and this shielding effect determines a reduction of the parameter A.

The eq. 5 lets define the conditions in which the system response to either the attenuation or the dephasing is maximized:

$$\left|\frac{\partial f}{\partial A}\right| = |\sin(\varphi - \theta)| \tag{6}$$

is maximal for $\phi = \varphi - \theta = \pi/2$, while

$$\left|\frac{\partial f}{\partial \theta}\right| = |A\cos(\varphi - \theta)| \tag{7}$$

is maximal when J_1 is maximum, that is at $\xi \approx 1.84$, and $\phi = 0, \pi$. These relations provide an indication of good experimental working conditions.

4. Results

The B_t variation due to the eddy currents induced in the specimen can be evaluated analytically for large (infinite radius) disks [28], or numerically for finite radius ones. The variation is monotonically dependent on the disk radius, and concerns both the phase and the amplitude of B_t. This is verified experimentally as shown in Fig. 3.

The atomic resonance is experimentally analyzed by scanning the frequency of the pump-laser modulation around the effective Larmor frequency expressed by the eq. 5. The resonance line-width is about 25 Hz, however the high S/N ratio let a best fit targeted to a Lorentzian profile determine the peak frequency with a sub-Hz accuracy. On the other hand, the ambient field fluctuations (the BB magnetometer is operated in an unshielded environment, with deactivated field-stabilization system [29]) are at nT level, and this leads to a few Hz uncertainty in the resonant frequency estimation.

The measurements shown here are performed at $B_0 = 1.7$ μT corresponding to an undressed Larmor frequency of 6 kHz. The dressing field frequency is set at 15 kHz or 30 kHz, and its amplitude B_D is set to get a dressing parameter $\xi = 1.84$, according to the indication provided by the eq. 7. In these conditions, the dressed frequency with no tuning field is $f_0 = J_0(1.84)\gamma B_0/2\pi \approx$ 1900 Hz.

Optics EXPRESS

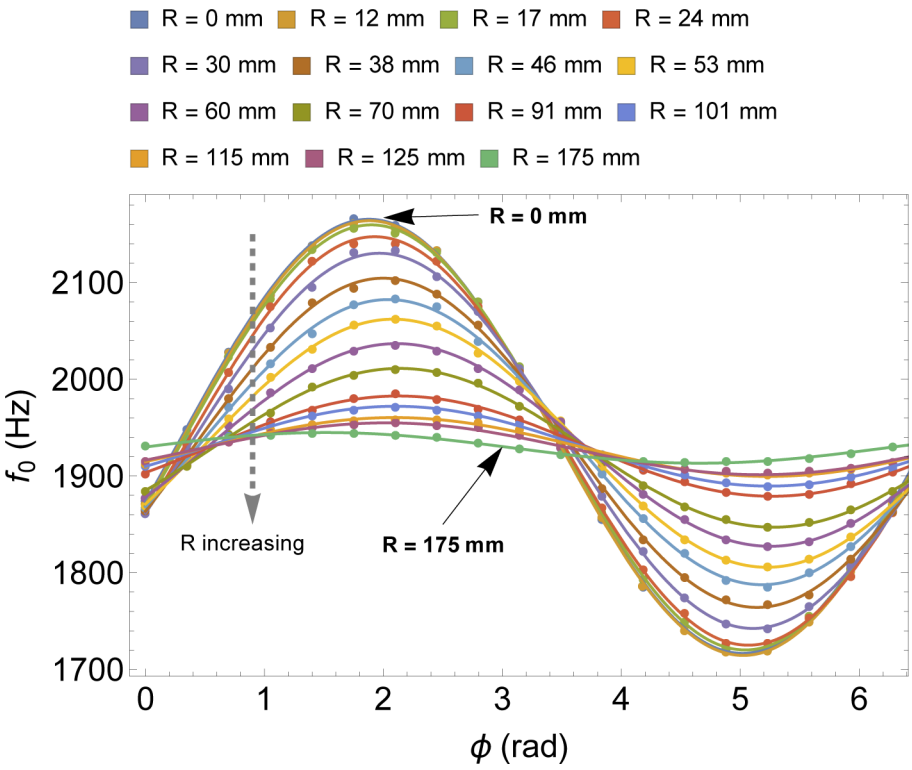

Fig. 3. The resonance frequency as a function of the different relative phase φ, for various disk diameters whose size in mm is reported in the legend. The vertical error bar (≈ 3 Hz) is smaller than the symbols used in the graph. The solid lines represent the best fit profile obtained with the target function eq. 5, with A and θ as fitting parameters.

When the tuning field is activated, the measured peak frequency has a remarkable dependence on both the amplitude and the phase of B_t at the sensor location, according to eq. 5. Both A and θ can be determined by scanning the relative phase of the RF generators in the $[0, 2\pi]$ interval.

The Fig. 3 shows clearly that an increase in disk radius causes both a reduction of the amplitude A and a phase shift of the sinusoidal profiles. It is also clear that larger variations of the effective Larmor frequency occur when $\phi = \pm\pi/2$, while operating near the zero-crossings ($\phi = 0, \pi$) improves the sensitivity to ϕ (i.e. to θ) variations, consistently with the eqs. 6, 7.

A clearer visualization is facilitated by a best fit procedure targeted to the function expressed in eq. 5. Plots of the best-fit parameter A versus the disk radius are shown with dots in Fig. 4, where the $A(R)$ parameter is normalized to its value $A(0)$ estimated in the absence of disks. The solid lines in that figure are results from finite element simulations. The latter is based on the geometry of Fig. 2, without the C_D solenoid and considering B_t at the center of the sensor as produced by a point dipolar source and attenuated by on axis Al disks.

This analysis has been performed with the set of Al disks described in Sec.2. and we report results obtained at both the tested tuning-dressing frequencies. Selecting different values of the oscillating fields changes the skin depth and hence modifies the shielding properties of the Al samples. As known, the skin depth depends on the absolute permeability μ of the medium and on its resistivity ρ, according to:

$$\delta = \sqrt{\frac{2\rho}{p\omega_D\mu}} \tag{8}$$

Optics EXPRESS

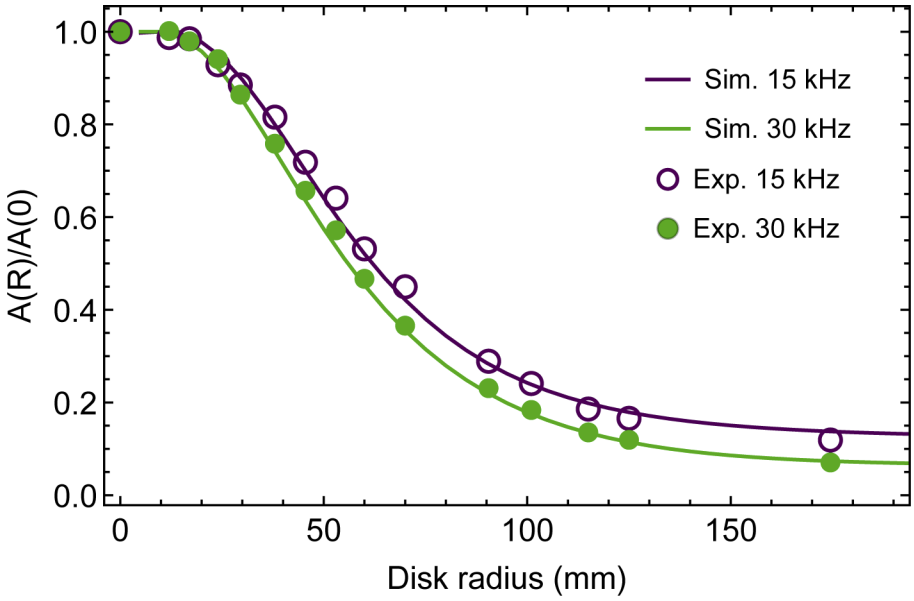

Fig. 4. Dependence of the tuning field amplitude (parameter A in eq. 5) on the Al disk radius R. The quantity is normalized to its value in the absence of disks. Both experimental data (dots) and results of a simplified numerical simulation (solid line, see text for more details) are reported. Both the cases of $\omega_D = 2\pi\cdot 15$ kHz and $2\pi\cdot 30$ kHz are considered. As expected, the larger is the disk, the stronger is the attenuation. Moreover, a thinner skin depth (data at 30 kHz) causes the amplitude decay faster and to a lower level, when the disk radius increases.

In the case of Al, this formula gives $\delta = 460$ μm and 650 μm, for the two considered frequencies, respectively. Both values are much larger than the thickness (30 μm) of the foil from which the Aluminum disks are cropped.

The general trend of the experimental results reported in Fig. 4 is qualitatively reproduced by numerical simulation. In particular both the experiment and the simulation show that the curve width and the asymptotic values decrease at higher ω_D (smaller δ). However, some quantitative discrepancies emerge: double thickness Al disks are considered in the simulation to produce the well matching profiles reported in Fig. 4. Indeed, several details are neglected in the simulation, such as the presence of the solenoid C_D and of an electric heater surrounding the Cs cell, and the finite size of the B_t source and of the sensor volume. Very likely, one or more of these factors are responsible for the mentioned discrepancies. Similar issues are encountered in the phase estimations $\theta(R)$.

5. Discussion

Our work addresses a novel detection scheme that could be used for imaging applications. Our main aim is to demonstrate the detection capabilities of the tuning-dressing technique under a controlled but not optimized geometry. The optimization issues related to reciprocal positions of sample, field generator, and detector, just to name few, are not analyzed. Those aspects are however essentially the same that apply in the case of other detection techniques. A complete and detailed analysis considering also the sample thickness as well as the other relevant parameters is beyond the scope of this paper. For this reason, the presented data consider only R variations for an assigned d.

Optics EXPRESS

An interesting feature (shared with other non-inductive detectors) is the extension to the low frequency range, while the non-resonant nature of the proposed scheme is innovative and constitutes an added value in this perspective.

The proposed tuning-dressing technique, extends to all-optical atomic magnetometric sensors applicability as detectors in EII setups. Interestingly, the proposed arrangement could be easily implemented in pre-existing EII apparatuses, and dual modality (RF and tuning-dressing) setups could be built, with incremental complexity of the available instrumentation.

In arrangements where the pump and probe beams are not parallel, a dual-mode operation would make possible to apply the RF field along different orientations, in such a way to induce variously distributed eddy currents. In fact, while in RF magnetometry the RF field is applied perpendicularly to the pump beam, in the tuning-dressing BB arrangement B_t is perpendicular to the probe beam.

Compared to conventional RF apparatuses, the tuning-dressing implementation enables fast selection of different B_t frequencies, via an appropriate selection of the harmonic parameter p. The possibility of selecting arbitrary values for both ω and p is relevant for the skin depth dependence on $p\omega_D$ (eq. 8), which is of interest to improve the tomographic (three-dimensional) potential of the EII apparatuses. In the case of RF magnetometers, changing the operation frequency requires the static field to be varied accordingly, to preserve the resonant condition. In practical applications, such variation may come with changes of its inhomogeneities, with the consequent need of gradient compensation.

Concerning the detection efficiency, the proposed methodology takes advantage from the fact that in the tuning-dressed configuration the weak tuning field borrows strength from the stronger dressing field. The linear dependence on B_t occurring for odd p (which can be maximized with appropriate choices of ξ and selecting $\phi = \pm\pi/2$) makes possible and efficient the use of approaches as that described in Ref. [2]. Specifically, it would be possible to apply a vanishing B_t obtained as a superposition of two opposite contributions, in such way that the specimen causes a B_t variation via an unbalance of the two applied terms.

Increasing the amplitude of the primary field is a straightforward method to improve the system sensitivity. Saturation effects [30] constitute a fundamental limit to this approach. Interestingly, the saturation limit of the primary field is set by different physical mechanisms in the cases of RF and tuning-dressing magnetometers, respectively. Namely, the latter require that eq. 4 is fulfilled, meaning that the saturation limit can be raised by strengthening B_D.

Improved detection techniques could be developed on the basis of the harmonic dependence on ϕ. As an example, if B_t oscillates at frequency ω_t slightly different from $p\omega$, the signal will appear as a low-frequency beating term oscillating at $\omega_t - p\omega$: a feature that would enable the application of phase-sensitive detection techniques.

6. Conclusion

We have presented a proof of principle experiment proposing a new kind of magnetometric detector of small or weakly conductive specimens. Specifically, we have used a recently studied dressing-field configuration to make an all-optical Bell-and-Bloom magnetometer suited to detect faint oscillating fields as occurring in magnetic induction tomography setups. The experiment demonstrated that the variation of a non-resonantly oscillating probe field can be effectively measured to detect the presence of conductive objects. The described approach can be regarded as non-resonant alternative to the well known methodologies based on RF magnetometers. It constitutes indeed a complementary approach to the problem and dual-mode (RF and tuning-dressing) apparatuses can be envisaged, with interesting novel features and enhanced flexibility in terms of interaction geometry and operation conditions: the proposed detection scheme enables the use of primary fields with different orientations and with an extended range of intensities and frequencies.

Optics EXPRESS

Further research is planned to validate the potential of the proposed detection technique in the reconstruction of EII maps and to study its performance in dependence on other relevant parameters.

Disclosures. The authors declare no conflicts of interest.

Data availability. Data underlying the results presented in this paper are not publicly available at this time but may be obtained from the authors upon reasonable request.

References

1. H. Griffiths, "Magnetic induction tomography," Meas. Sci. Technol. **12**(8), 1126–1131 (2001).
2. C. Deans, L. Marmugi, and F. Renzoni, "Sub-Sm^{-1} electromagnetic induction imaging with an unshielded atomic magnetometer," Appl. Phys. Lett. **116**(13), 133501 (2020).
3. Z. Z. Yu, A. T. Peyton, M. S. Beck, W. F. Conway, and L. A. Xu, "Imaging system based on electromagnetic tomography (EMT)," Electron. Lett. **29**(7), 625–626 (1993).
4. A. Korjenevsky, V. Cherepenin, and S. Sapetsky, "Magnetic induction tomography: experimental realization," Physiol. Meas. **21**(1), 89–94 (2000).
5. P. Bevington, R. Gartman, and W. Chalupczak, "Inductive imaging of the concealed defects with radio-frequency atomic magnetometers," Appl. Sci. **10**(19), 6871 (2020).
6. M. Soleimani, W. R. B. Lionheart, and A. J. Peyton, "Image reconstruction for high-contrast conductivity imaging in mutual induction tomography for industrial applications," IEEE Trans. Instrum. Meas. **56**(5), 2024–2032 (2007).
7. L. Ma and M. Soleimani, "Magnetic induction tomography methods and applications: a review," Meas. Sci. Technol. **28**(7), 072001 (2017).
8. A. Wickenbrock, S. Jurgilas, A. Dow, L. Marmugi, and F. Renzoni, "Magnetic induction tomography using an all-optical ^{87}Rb atomic magnetometer," Opt. Lett. **39**(22), 6367–6370 (2014).
9. A. Wickenbrock, N. Leefer, J. W. Blanchard, and D. Budker, "Eddy current imaging with an atomic radio-frequency magnetometer," Appl. Phys. Lett. **108**(18), 183507 (2016).
10. Y. Cohen, K. Jadeja, S. Sula, M. Venturelli, C. Deans, L. Marmugi, and F. Renzoni, "A cold atom radio-frequency magnetometer," Appl. Phys. Lett. **114**(7), 073505 (2019).
11. A. Fregosi, C. Gabbanini, S. Gozzini, L. Lenci, C. Marinelli, and A. Fioretti, "Magnetic induction imaging with a cold-atom radio frequency magnetometer," Appl. Phys. Lett. **117**(14), 144102 (2020).
12. G. Chatzidrosos, A. Wickenbrock, L. Bougas, H. Zheng, O. Tretiak, Y. Yang, and D. Budker, "Eddy-current imaging with nitrogen-vacancy centers in diamond," Phys. Rev. Appl. **11**(1), 014060 (2019).
13. Y. Tavrin, H.-J. Krause, W. Wolf, V. Glyantsev, J. Schubert, W. Zander, and H. Bousack, "Eddy current technique with high temperature SQUID for non-destructive evaluation of non-magnetic metallic structures," Cryogenics **36**(2), 83–86 (1996).
14. N. Tralshawala, J. R. Claycomb, and J. H. Miller, "Practical SQUID instrument for nondestructive testing," Appl. Phys. Lett. **71**(11), 1573–1575 (1997).
15. C. H. Smith, R. W. Schneider, T. Dogaru, and S. T. Smith, "Eddy-current testing with GMR magnetic sensor arrays," AIP Conf. Proc. **700**, 406–413 (2004).
16. L. S. Rosado, F. A. Cardoso, S. Cardoso, P. M. Ramos, P. P. Freitas, and M. Piedade, "Eddy currents testing probe with magneto-resistive sensors and differential measurement," Sensors and Actuators A: Physical **212**, 58–67 (2014).
17. J. Bailey, N. Long, and A. Hunze, "Eddy current testing with giant magnetoresistance (GMR) sensors and a pipe-encircling excitation for evaluation of corrosion under insulation," Sensors **17**(10), 2229 (2017).
18. C. Deans, L. Marmugi, S. Hussain, and F. Renzoni, "Electromagnetic induction imaging with a radio-frequency atomic magnetometer," Appl. Phys. Lett. **108**(10), 103503 (2016).
19. V. Gerginov, "Field-polarization sensitivity in rf atomic magnetometers," Phys. Rev. Appl. **11**(2), 024008 (2019).
20. K. Jensen, M. Zugenmaier, J. Arnbak, H. Stærkind, M. V. Balabas, and E. S. Polzik, "Detection of low-conductivity objects using eddy current measurements with an optical magnetometer," Phys. Rev. Res. **1**(3), 033087 (2019).
21. L. Marmugi, C. Deans, and F. Renzoni, "Electromagnetic induction imaging with atomic magnetometers: Unlocking the low-conductivity regime," Appl. Phys. Lett. **115**(8), 083503 (2019).
22. H. Scharfetter, R. Casanas, and J. Rosell, "Biological tissue characterization by magnetic induction spectroscopy (MIS): requirements and limitations," IEEE Trans. Biomed. Eng. **50**(7), 870–880 (2003).
23. G. Bevilacqua, V. Biancalana, Y. Dancheva, A. Fregosi, and A. Vigilante, "Spin dynamic response to a time dependent field," Appl. Phys. B **127**(9), 128 (2021).
24. S. Haroche, C. Cohen-Tannoudji, C. Audoin, and J. P. Schermann, "Modified Zeeman hyperfine spectra observed in ^{1}H and ^{8}7Rb ground states interacting with a nonresonant RF field," Phys. Rev. Lett. **24**(16), 861–864 (1970).
25. G. Bevilacqua, V. Biancalana, A. Vigilante, T. Zanon-Willette, and E. Arimondo, "Harmonic fine tuning and triaxial spatial anisotropy of dressed atomic spins," Phys. Rev. Lett. **125**(9), 093203 (2020).
26. G. Bevilacqua, V. Biancalana, P. Chessa, and Y. Dancheva, "Multichannel optical atomic magnetometer operating in unshielded environment," Appl. Phys. B **122**(4), 103 (2016).
27. D. Cubero, L. Marmugi, and F. Renzoni, "Exploring the limits of magnetic field focusing: Simple planar geometries," Results Phys. **19**, 103562 (2020).

Optics EXPRESS

28. C. V. Dodd and W. E. Deeds, "Analytical solutions to eddy-current probe-coil problems," J. Appl. Phys. **39**(6), 2829–2838 (1968).
29. G. Bevilacqua, V. Biancalana, Y. Dancheva, and A. Vigilante, "Self-adaptive loop for external-disturbance reduction in a differential measurement setup," Phys. Rev. Appl. **11**(1), 014029 (2019).
30. H. Yang, Y. Wang, and N. Zhao, "Saturation effect of atomic magnetic resonance," AIP Adv. **10**(5), 055013 (2020).